Clocking the social mind by identifying mental processes in the IAT with electrical neuroimaging

Bastian Schiller[a,b,c,1,2], Lorena R. R. Gianotti[b,c,d,1,2], Thomas Baumgartner[b,c,d], Kyle Nash[b,c,d], Thomas Koenig[d,e], and Daria Knoch[b,c,d,2]

[a]Department of Psychology, Laboratory for Biological and Personality Psychology, University of Freiburg, DE-79104, Freiburg, Germany; [b]Institute of Psychology, Department of Social Psychology and Social Neuroscience, University of Bern, CH-3012, Bern, Switzerland; [c]Department of Psychology, Social and Affective Neuroscience, University of Basel, CH-4055, Basel, Switzerland; [d]Center for Cognition, Learning and Memory, University of Bern, CH-3012, Bern, Switzerland; and [e]Translational Research Center, University Hospital of Psychiatry, University of Bern, CH-3000, Bern, Switzerland

Edited by Susan T. Fiske, Princeton University, Princeton, NJ, and approved January 12, 2016 (received for review August 11, 2015)

Why do people take longer to associate the word "love" with outgroup words (incongruent condition) than with ingroup words (congruent condition)? Despite the widespread use of the implicit association test (IAT), it has remained unclear whether this IAT effect is due to additional mental processes in the incongruent condition, or due to longer duration of the same processes. Here, we addressed this previously insoluble issue by assessing the spatiotemporal evolution of brain electrical activity in 83 participants. From stimulus presentation until response production, we identified seven processes. Crucially, all seven processes occurred in the same temporal sequence in both conditions, but participants needed more time to perform one early occurring process (perceptual processing) and one late occurring process (implementing cognitive control to select the motor response) in the incongruent compared with the congruent condition. We also found that the latter process contributed to individual differences in implicit bias. These results advance understanding of the neural mechanics of response time differences in the IAT: They speak against theories that explain the IAT effect as due to additional processes in the incongruent condition and speak in favor of theories that assume a longer duration of specific processes in the incongruent condition. More broadly, our data analysis approach illustrates the potential of electrical neuroimaging to illuminate the temporal organization of mental processes involved in social cognition.

implicit social cognition | social neuroscience | intergroup bias | ERP | microstates

From the beginning of psychological research, reaction times have been used to probe the nature of mental processes, an approach known as mental chronometry (1, 2). This experimental approach has led to the development of dozens of psychological tests (e.g., Stroop tasks, priming tasks, implicit association tests) that rely on response time differences to assess implicit, unconscious processes (3–5). These response time differences provide unique information that predicts behavior, judgments, physiological responses, and pathology (6, 7). One of the most popular of these tests is the implicit association test (IAT; refs. 8 and 9). The IAT measures implicit attitudes or gut-level evaluations, such as attitudes about different social groups. It is based on the idea that participants are slower at associating incongruent vs. congruent stimuli, a reaction time difference known as the "IAT effect." For example, participants usually take longer to associate ingroup words with negative attributes (incongruent condition) than with positive attributes (congruent condition), indicating that they hold positive attitudes toward their ingroup.

Despite the widespread use of the IAT, it is still unclear why participants take longer to respond in the incongruent condition. There are two main possible explanations. It could be that additional mental processes are needed in the incongruent condition to solve the task correctly, for instance inhibiting automatic evaluations (e.g., negative evaluation of the outgroup) that interfere with the correct response (e.g., associate outgroup words with positive attributes; ref. 10). Alternatively, the same mental processes may be performed in both conditions, but participants could need more time to perform one or a number of them in the incongruent condition, for instance, selecting a motor response (11).

To illuminate which of these two explanations accounts for the IAT effect, it is necessary to identify and time the entire chain of mental processes involved in executing the IAT. Mental processes are mediated by large-scale neural networks linking groups of neurons in separate cortical areas into functional entities (12–14). Activity in these neural networks can be studied with millisecond resolution by using a spatiotemporal analysis of multichannel electroencephalogram (EEG). By segmenting electrical activity recorded during execution of the IAT into time periods of stable neural network configurations, one can identify functional microstates of the brain that each represent the implementation of a specific mental process (15–17). Capitalizing on such an integrative analysis of space and time information of the EEG data, here, we wished to identify all mental processes involved during the execution of the IAT and to precisely measure the duration of all these processes by determining their onset and offset in time.

To illustrate the value of our approach, consider the following example: Much like comparing the mental processes in the incongruent and the congruent IAT conditions to reveal why participants take longer to respond in the incongruent condition, you might compare your activities on a Monday with your activities on a Friday to reveal why you went to bed later on Friday. There are two possible reasons for why you went to bed later on

Significance

What a person says is not necessarily an accurate representation of what she thinks. Implicit attitudes permeate every aspect of our life. The implicit association test (IAT)—the most well-known test of implicit attitudes—is a reaction time measure. So far, the fundamental question about the source of its reaction time differences, i.e., the IAT effect, has remained unanswered. For the first time to our knowledge in IAT research, we applied a sophisticated electrical neuroimaging approach—the microstate approach. Superior to other approaches, the microstate approach allowed us to identify and time the entire chain of mental processes as they unfolded during the IAT. We found that reaction time differences are due to quantitative and not qualitative differences in the underlying mental processes.

Author contributions: B.S., L.R.R.G., T.B., T.K., and D.K. designed research; B.S. and L.R.R.G. performed research; B.S., L.R.R.G., T.B., and T.K. analyzed data; and B.S., L.R.R.G., K.N., and D.K. wrote the paper.

The authors declare no conflict of interest.

This article is a PNAS Direct Submission.

[1]B.S. and L.R.R.G. contributed equally to this work.

[2]To whom correspondence may be addressed. Email: daria.knoch@psy.unibe.ch, schiller@psychologie.uni-freiburg.de, or lorena.gianotti@psy.unibe.ch.

This article contains supporting information online at www.pnas.org/lookup/suppl/doi:10.1073/pnas.1515828113/-/DCSupplemental.

Friday: You might have performed a unique activity on Friday (e.g., having a drink with some friends in the evening) that you did not do on Monday and this activity delayed your bed time. Or you might have performed the same activities for a different duration. For instance, in the evening you might have watched television (TV) longer on Friday than on Monday, delaying the time you went to bed. To better understand the origin of such duration differences, it might also be informative to consider whether these differences are driven by differences in the intensity of previous activities. For example, it could be that on Monday you had worked harder than on Friday. As a consequence, you became tired much earlier and watched TV for a shorter duration before you went to bed.

Previous EEG studies have reported differences in event-related potentials (ERPs) between IAT conditions both at early (in the first half of task execution; refs. 18–21) and at late time periods (in the second half of task execution; refs. 18, 19, and 22–24). Thus, differences in both early and late mental processes appear to produce the IAT effect. None of these studies, however, has exploited the full amount of spatiotemporal information available from ERP data. Rather, they have compared ERPs between the two IAT conditions at identical predefined time points, yielding inconclusive evidence about why participants take longer to respond in the incongruent condition. Recall our day-activities example. Imagine that we compare activities between Monday and Friday late in the evening. On Monday, you were watching TV, and on Friday, you were having a drink with some friends. However, is it because you were having a drink that you went to bed later on Friday? Maybe, you had a quick drink on Monday as well, before watching TV. Obviously, you need to consider more than just the late evening. Only a comprehensive analysis of the full range of activities you performed during both days will unambiguously shed light on the reason why you went to bed later on Friday. Similarly, only a comprehensive analysis of the continuous flow of all mental processes occurring between stimulus presentation and response production will unambiguously shed light on the IAT effect.

Therefore, we used a data-driven, spatiotemporal EEG microstate analysis approach that allows identifying and timing all mental processes involved in executing the IAT. We analyzed data from 83 participants (37 soccer fans and 46 political supporters) who performed an ingroup/outgroup IAT. By identifying the series of mental processes during execution of both IAT conditions, we were able to reveal whether the IAT effect is due to additional, unique mental processes or longer, identical mental processes in the incongruent condition. Moreover, we localized the intracranial brain sources that underlie each mental process to ascertain which brain areas are activated when performing the task. Such information allows for speculation about the nature of differences between the two conditions in the stream of mental processing during IAT performance.

Results

Behavior. On average, participants performed at 95% accuracy in the incongruent condition and at 98% accuracy in the congruent condition [errors incongruent: mean (M) = 14.06, standard deviation (SD) = 10.00; errors congruent: M = 6.84, SD = 6.40; $t(82) = 9.16$, $P < 0.001$, $\eta^2 = 0.51$]. Comparing reaction times in incongruent trials (M = 853.10 ms, SD = 93.56 ms) to those in congruent trials (M = 734.87 ms, SD = 95.83 ms) revealed the classical IAT effect with prolonged reaction times in incongruent trials [$t(82) = 14.88$, $P < 0.001$, $\eta^2 = 0.73$]. The IAT effect was present both in soccer fans [$t(36) = 11.95$, $P < 0.001$, $\eta^2 = 0.80$] and in political supporters [$t(45) = 9.66$, $P < 0.001$, $\eta^2 = 0.68$].

ERPs and Microstate Analysis.

Is the IAT effect explained by additional processes in the incongruent condition? Based on a silhouette plot, we identified nine clusters that explained 92% of the variance in the data (Fig. S1). The cluster solution with nine clusters was chosen because all clusters had a reasonable structure (silhouette values >0.50). The topographies of the nine clusters are depicted in Fig. 1*A* (see *SI Results* for a detailed description of these nine topographies). Fitting the clusters to each grand-mean ERP by means of spatial correlation demonstrated an identical sequence of nine microstates (i.e., mental processes) for both conditions between 0 and 1,000 ms (Fig. 1*B*). Because two of these microstates occurred after the mean button press, we focus on the seven microstates that occurred between stimulus onset and button press.

Importantly, there were no additional microstates in the incongruent condition, indicating that additional mental processes in the incongruent condition were not causing the longer reaction times in this condition. To assess the robustness of these findings, we compared results between soccer fans and political supporters by rerunning the topographic fitting procedure separately for each group. The sequence of microstates was identical for both groups, and there were no additional microstates in the incongruent condition for either soccer fans or political supporters, indicating that our results apply beyond a specific population performing a specific IAT version (Fig. S2). Also, the same sequence of microstates was found when separately rerunning the cluster and topographic fitting procedures in participants with large and small implicit bias (based on a median split, see Fig. S3).

Do participants take longer to perform certain processes in the incongruent condition? Because the IAT effect could not be explained by additional microstates in the incongruent condition, we next examined microstate durations in the incongruent compared with the congruent condition. We found that two microstates, microstate 4 (starting around 220 ms) and microstate 6 (starting around 450 ms) were prolonged in the incongruent condition (microstate 4: $M_{inc} = 34$ ms, $M_{con} = 28$ ms, $P = 0.0014$; microstate 6: $M_{inc} = 218$ ms, $M_{con} = 170$ ms, $P < 0.001$; Fig. 1*B* and Table 1). Thus, duration differences in microstates 4 and 6 contribute to the IAT effect.

Do differences in the intensity of previous processes contribute to the duration differences? Recall from our example in the Introduction that differences in the duration of microstates might be driven by differences in the intensity of previous microstates. We tested this possibility with regard to all microstates that preceded the two microstates in which duration differences were found, i.e., microstates 4 and 6. We found that differences in the intensity of microstate 3 ($M_{inc} = 1.67$ μV, $M_{con} = 1.55$ μV, $P < 0.001$) modulated differences in the duration of the subsequent microstate 4: The more intense microstate 3 was, the longer microstate 4 took in the incongruent than the congruent condition ($r = 0.29$, $P < 0.01$). No other microstate intensity difference modulated the durations of microstate 4 or microstate 6 ($P > 0.13$).

Do individual differences in the duration of processes help explain individual differences in implicit bias? Correlational analyses revealed that the duration of microstate 6 contributed to individual differences in implicit bias: Increased time spent in microstate 6 in the incongruent compared with the congruent condition was associated with an increased implicit bias [$r(81) = 0.25$, $P = 0.021$]. Individual differences in the duration of all other microstates did not correlate with implicit bias (all r values $<|0.09|$, P values >0.20).

Source Localization. In a final step, we source localized microstates 3, 4, and 6 to get an idea about the nature of each mental process that accounts for the IAT effect (Fig. 1*C*; for a detailed description of source localization results of all microstates, see *SI Results*, Table S1, and Fig. S4). Microstate 3 was characterized by activity in the left temporal pole (BA22/38), the left insula (BA13), and the dorsal anterior cingulate cortex (dACC; BA24). Microstate 4 was characterized by activity in the lingual gyrus (BA18) and other occipitotemporal areas. Finally, microstate 6 was characterized by activity in the middle cingulate cortex (MCC; BA23/24/31) and the posterior parietal cortex (PPC; BA40).

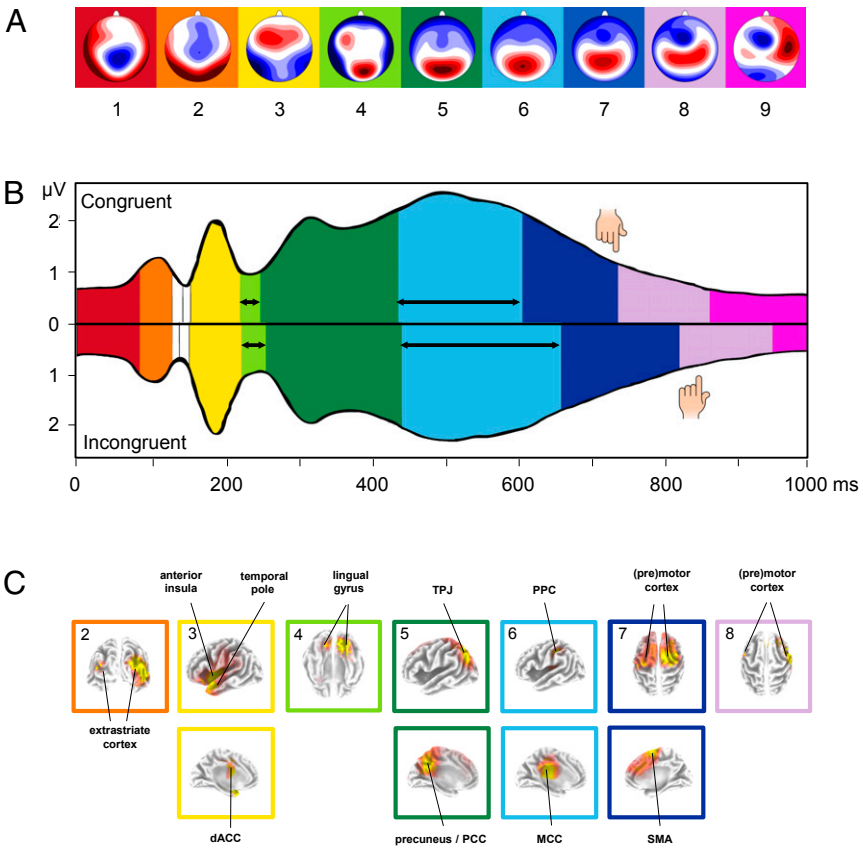

Fig. 1. Microstate analysis of the IAT-evoked ERPs. (*A*) Topographies of the nine microstate clusters in the sequence of occurrence. Head seen from above: Red indicates positive values and blue negative values, referred to average reference. The colored background corresponds to the assignment shown in *B* and *C*. (*B*) Microstates across time for the congruent (*Upper*) and incongruent condition (*Lower*) plotted over the Global Field Power (GFP). Colors refer to the microstate topographies shown in *A*. The hand symbols indicate mean response times. The vertical axis indicates GFP (in microvolts); the horizontal axis indicates time (in milliseconds). Black horizontal arrows indicate microstates in which significant, Bonferroni-corrected duration differences were observed between IAT conditions ($P < 0.001$). Note that we only considered microstates that lasted for at least 10 ms (shorter microstates are shown in white). (*C*) Localization of the intracortical sources as estimated with sLORETA for the full sequence of microstates during the IAT. Bonferroni-corrected, significant voxels are colored, with increasing *t* values from red to yellow. Note that, for each microstate, the grading of colors was adapted to accentuate the main activation clusters, such that identical colors in different microstates do not represent identical *t* values. We labeled the main activation clusters and framed the localization with the same color code as the corresponding microstates in *A* and *B*. Please note that intracortical sources are only shown for microstates 2–8 due to the chosen source localization strategy (for details, see *SI Materials and Methods* and *SI Results*). PCC, posterior cingulate cortex; SMA, supplementary motor area; TPJ, temporo-parietal junction.

Discussion

The main goal of this study was to explain why participants completing the IAT take longer to respond in the incongruent compared with the congruent condition. Do additional mental processes occur in the incongruent condition? Or do participants just need more time to perform one or a number of mental processes in the incongruent condition? Also, if we know which of these two explanations is true, then what are the mental processes that differ between IAT conditions? This study was conducted to reveal the mental processes that underlie the most-used measure of implicit cognition by directly observing brain areas that are activated when performing the task.

Several theoretical proposals (Differential Task Switching model, ref. 25; Quadruple Process model, ref. 10; Random Walk model, ref. 26; Response Activation account, ref. 11) articulate specific mental processes in the IAT effect. However, so far, no study has empirically examined the full range of mental processes that occur during the two IAT conditions. By using a data-driven, comprehensive ERP analysis procedure (microstate approach) combined with source localization, we were able to identify and to precisely time all mental processes involved during IAT performance. From stimulus onset until response implementation, we identified seven mental processes. Crucially, all seven processes occurred in the same temporal sequence in both conditions, in direct contrast to the possible explanation that additional, unique mental processes in the incongruent condition would explain the longer reaction times. The main theoretical proposal that explicitly takes into account an additional, unique mental process in the incongruent condition is the Quadruple Process model (10). According to this model, an additional inhibitory process is needed in the incongruent condition to overcome automatic evaluations of the stimulus that are incompatible with the correct response. Previous studies applying the Quadruple Process model to the IAT, however, have yielded equivocal results (10, 27, 28). Capitalizing on the microstates approach, we did not find evidence for the existence of an additional process during the incongruent condition. Rather, we found support for the alternative explanation of the IAT effect: Participants needed more time to perform certain mental processes in the incongruent compared with the congruent condition.

More precisely, we identified two mental processes that lasted longer in the incongruent condition and, thus, produced the IAT effect. The first duration difference was found in an early mental process, starting around 220 ms after stimulus onset (microstate 4). The second was found in a later mental process, starting around 450 ms after stimulus onset (microstate 6). Thus, in line with previous EEG studies, we found differences between the two IAT conditions in both the first (18–21) and second half (18, 19, 22–24) of task execution. Adding to previous research, we demonstrated that these differences were due to a longer duration of the same mental

Table 1. Descriptive onsets and offsets of microstates in milliseconds

	1		2		3		4		5		6		7		8	
Microstate	On	Off	On	Off	On	Off	On	Off	On	Off	On	Off	On	Off	On	Off
Congruent	0	88	88	132	158	224	224	252	252	442	442	612	612	742	742	868
Incongruent	0	88	88	132	156	226	226	260	260	446	446	664	664	826	826	954

processes in the incongruent condition. Recall again our day-activities example. Comparing your activities between Monday and Friday at a specific moment in time (e.g., the late evening) without considering the rest of the day reveals that on Friday you had a drink with some friends whereas on Monday you watched TV. However, the question about why you went to bed later on Friday remains unanswered. By considering the full range of activities you performed during both days, perhaps you realize that you had a drink with friends and watched TV on both Monday and Friday, but on Friday you spent more time doing these activities.

What can we tell about the two mental processes that lasted longer in the incongruent condition? Based on the neural generators of microstate 4 (lingual gyrus and other vision-related areas) and on its time of appearance, we speculate that participants processed the presented words during this microstate, extracting orthographical and phonological information (29, 30). Why should the same words need longer perceptual processing in the incongruent condition? Considering the preceding mental process (executed during microstate 3) may help to answer this question: The neural generators of microstate 3 (left temporal pole, the left insula, and the dACC) combined with its time of appearance suggest that arousal-related processing takes place during this microstate (31, 32). Previous studies have shown that arousal can modulate subsequent perceptual processing (33, 34). Based on this idea and given that arousal-related processing during microstate 3 was enhanced in the incongruent condition, we tested whether such enhanced processing might drive the subsequent prolongation of perceptual processing during microstate 4. Indeed, we could confirm this assumption. At first glance, the positive link between intensity of microstate 3 and duration of microstate 4 might seem counterintuitive because one could expect that higher arousal should lead to more efficient (i.e., faster) perceptual processing. However, we argue that the enhanced arousal-related processing in the incongruent condition signals the need for more careful (longer) subsequent perceptual processing. Additional evidence from brain stimulation studies substantiates this idea. Transiently disrupting the temporal pole (which we found to be involved in the arousal-related microstate 3) causes a diminished response time difference in the IAT, mainly by accelerating responses in the incongruent condition (35, 36). Future studies could combine single-pulse transcranial magnetic stimulation with EEG to test whether disrupting activity in the temporal pole during the arousal-related process in the incongruent condition causes a shortening of the subsequent perception-related process.

The second duration difference occurred in microstate 6. On average, participants needed 50 ms longer to perform this mental process in the incongruent condition compared with the congruent condition. The neural generators of microstate 6 (MCC and PPC) combined with its time of appearance and its position in the sequence of microstates leads us to assume that participants implement cognitive control to select the motor response during this microstate (37–39). Our interpretation is validated by the next microstate that appears immediately before button press. Its characteristic neural generators encompass motor-related frontal regions (premotor cortex, supplementary motor area, and primary motor cortex), indicating that the motor response is executed during this microstate (time of button press is indicated by hand symbols in Fig. 1*B*). The fact that microstate 6 was present during the incongruent and the congruent condition indicates that participants require cognitive control to select between the two response options in all trials. However, during the incongruent condition, participants require more control (i.e., need longer) to select the correct motor response presumably because the competition between the two response options is stronger. This interpretation is in line with the Response Activation account of the IAT effect (11), according to which selecting the correct motor response is more difficult and takes longer in the incongruent condition. The competition between the two motor response options seems to be more difficult to resolve in people with stronger bias, as shown by the positive link between microstate 6 duration and implicit bias. The larger the implicit bias, the more time a participant spent selecting the correct motor response in the incongruent compared with the congruent condition. Overall, our results indicate that (*i*) both early and late processes contribute to the IAT effect and (*ii*) individual differences are mainly driven by a relatively late process, namely control in the selection of the correct motor response rather than by early processes.

In sum, by analyzing the whole time window and not—as previously done—focusing on only selected time windows or specific electrodes, we showed that the IAT effect cannot be explained by additional mental processes in the incongruent condition. Rather, we found that the IAT effect occurs because participants need more time to perform two mental processes in the incongruent condition. By using the microstate approach, we extended and reconciled some seemingly discrepant findings in the literature. We hope to have clarified that focusing on selected time windows leads to findings that are correct but partial. What ERP research needs is some means of integrating and reconciling their (perfectly valid, but incomplete) selective findings. The microstate approach used in the present study enables a comprehensive perspective in the study of the IAT effect and, more broadly, in the study of the psychological sources of response time differences, be it between different conditions of an experimental task (e.g., Stroop tasks, priming tasks), between treatment groups (e.g., brain stimulation, hormone administration), between patients and healthy controls, or between people of different ages. Integrating classic psychological theories with the investigation of neural bases using the microstate approach will benefit both psychologists and neuroscientists that are attempting to precisely clock the social mind.

Materials and Methods

Participants. We collected data from 84 right-handed and German speaking participants who were recruited from the University of Basel. Informed consent was obtained from all participants who were screened for health problems by using a detailed health questionnaire. Participants indicated neither current nor previous history of neurological and psychiatric disorders and alcohol and drug abuse. One participant had to be excluded from further analysis because of an excessive amount of EEG artifacts, leaving a sample of 83 participants (38 female and 45 male). Mean age was 21.9 y (SD = 3.0 y, range: 21–48 y). We recruited participants who had, on a scale from 1 (very weak) to 5 (very strong), at least medium (=3) self-reported interest in soccer or in politics, because previous studies using sport fans and political supporters have reported strong intergroup biases (40–42). We collected data from both soccer fans (n = 37) and political supporters (n = 46) to test whether our results are generalizable beyond a specific social group (43, 44). We measured each participant's identification strength with his or her favored soccer club or political party by using a modified version of the Sport Spectator Identification Scale (5-point Likert scale; ref. 45). We found that, on average, participants showed a medium to strong identification with their group (M = 3.39, SD = 0.58) and that there were no significant differences between soccer fans and political supporters [soccer fans: M = 3.50, SD = 0.59; political supporters: M = 3.35, SD = 0.55; soccer fans vs. political supporters: $t(80) = 1.15$, $P > 0.20$]. Participants received 30 Swiss francs (CHF 30; CHF 1 = 1$ U.S.) for participation. The Ethics Committee of Basel approved the study, which was conducted according to the principles expressed in the Declaration of Helsinki.

IAT. We used an IAT that measured implicit intergroup attitudes (8, 23). More specifically, we determined how strongly participants automatically associate their ingroup and outgroup with positive and negative valenced words. Participants were required to correctly and quickly classify words belonging to four categories: ingroup (e.g., names of soccer players of the favored soccer club), outgroup (e.g., names of soccer players of the rival soccer club), positive (e.g., "love") and negative (e.g., "death"). Please note that for each participant, we adapted the ingroup and outgroup words based on his or her preferred social group (see Table S2 for a complete list of stimuli used for the distinct social groups). Participants were instructed to pay attention to both accuracy and latency. Participants were also informed

that they would receive feedback via a red "X" in the middle of the screen if an incorrect response was recorded and that they could not correct their incorrect response. The words appeared in the middle of a personal computer screen in black letters against a white background, and participants were asked to assign the words by pressing one of two response keys with the left and right index finger, respectively. The rules of category-response assignments reversed from block to block, and the categories were presented throughout the block in the upper left and right hand corner of the screen. The IAT contained 10 blocks (364 trials in total). In the first two blocks (10 trials each), participants learned to classify positive vs. negative words and ingroup vs. outgroup words, respectively. In the third "congruent" block (76 trials) participants had to press one key when ingroup or positive words appeared and another key when outgroup or negative words were shown. In the fourth block, response assignments for positive and negative words were reversed (10 trials), so that in the fifth "incongruent" block (76 trials) ingroup and negative words shared the same response key, whereas outgroup and positive words shared another response key. After these first five blocks, participants had to do another five-block IAT, where the order of the congruent and incongruent block was switched. In each trial, the word was presented for 1,500 ms, followed by a screen where only the category labels were shown with a randomly jittered duration ranging from 2,000 to 2,200 ms, resulting in a mean stimulus onset asynchrony of 3,600 ms. The entire experiment lasted ~30 min.

Analysis of Behavioral Data. For each subject, we calculated mean reaction time and accuracy for the incongruent and congruent trials, respectively. The IAT effect is calculated by subtracting mean reaction times in the congruent condition from those in the incongruent condition. Only trials with correct responses occurring within 300–1,500 ms after stimulus presentation were used for all further analyses. The D scores reported in (*SI Results*) were calculated according to the improved scoring algorithm (46).

EEG Recording. During IAT completion, we recorded the EEG with a Biosemi ActiveTwo system from 64 Ag-AgCl active electrodes according to the 10–10 system montage (47). The signals were referenced online to the common mode sense, while driven right leg served as ground. Horizontal and vertical electrooculographic signals were recorded with two additional electrodes at the left and right outer canthi and one electrode at the left infraorbital. The EEG was online band-pass filtered between 0.1 and 100 Hz, and the data were digitized with a sampling rate of 512 Hz.

EEG Preprocessing. EEG data collected during the IAT were analyzed by using Brain Vision Analyzer (Version 2.0.1.391; Brain Products). Eye-movement artifacts were corrected by using an Independent Component Analysis. EEG signals with excessive noise were replaced by using a linear interpolation of adjacent electrodes. After an automatic artifact rejection (maximal voltage step: 50 μV; maximal amplitude difference in intervals of 150-ms length: 150 μV; maximal amplitude: $\pm$ 100 μV), data were visually examined to eliminate residual artifacts. Data were then band-pass filtered (no additional high-pass, low-pass 30 Hz) and rederived to average reference.

ERPs and Microstate Analysis. Using a time window from stimulus onset to 1,000 ms after (which is well beyond the known average response times of the IAT conditions; refs. 23 and 24), individual artifact-free ERPs were computed for the two conditions, one averaging all incongruent trials and one averaging all congruent trials. A mean of 135 congruent trials (SD = 20; minimum: 45) and 137 incongruent trials (SD = 21; minimum: 57) were available for averaging. Then, the individual ERPs were averaged into two grand-mean ERPs, one for each condition.

To identify sequences of time periods with quasistable scalp map topographies referred to as functional microstates (16, 17), the spatial K-means clustering approach was used (ref. 48; for alternative approaches, see ref. 49). This strategy uses global map dissimilarity (16) as a measure of topographical difference between any two maps. The spatial cluster analysis allowed us to define the most dominant topographies (i.e., clusters) in the grand-mean ERP map series of the incongruent condition and the grand-mean ERP map series of the congruent condition. The optimal number of clusters was selected with the silhouette analysis such that a maximum number is obtained while all clusters retain a reasonable structure, i.e., silhouette values more than 0.50 (50).

A topographic fitting procedure was applied to identify the resulting microstates in each condition (51). We applied the constraint that a given scalp map topography must be observed for at least five consecutive time points (>10 ms) in the grand-mean ERPs (see also ref. 52). Also, in our statistical analysis, we focused on those microstates that occurred before the button press.

In a second step, the clusters (as identified in the two grand-mean ERP map series) were fit back to the individual ERPs in each condition. Each time point is labeled with the cluster it correlated best with (in terms of global map dissimilarity), yielding a measure of cluster presence (in milliseconds) for each individual ERP in both conditions, separately.

As a final step, we estimated the intracerebral sources that gave rise to each of the microstates, using the standardized low-resolution brain electromagnetic tomography (sLORETA; ref. 53). The sLORETA algorithm has been widely used in many EEG studies (54–59). This method has been shown to outperform several other linear inverse algorithms (53) and has been extensively cross-validated (for details, see *SI Materials and Methods*).

Statistical Analyses. We compared mean reaction times for congruent and incongruent trials with paired *t* tests. Using randomization statistics (60, 61), we tested for significant differences in the duration of microstates between conditions. We only report results significant at 5% that survive Bonferroni correction.

To explain individual differences in implicit bias, we correlated the individual mean duration differences (between the two conditions) of each cluster with participants' implicit bias.

Finally, we investigated whether differences in the intensity of previous microstates contributed to duration differences (i.e., the influence of intensities of microstates 1–3 on the duration of microstate 4, and the influence of intensities of microstates 1–5 on the duration of microstate 6). To quantify differences in microstate intensity, we calculated the mean Global Field Power (GFP) during a microstate (refs. 16 and 62). GFP corresponds to the spatial SD of the electric field and, thus, yields a measure of global signal strength independent of topography.

ACKNOWLEDGMENTS. We dedicate this manuscript to the memory of Prof. Dietrich Lehmann, discoverer of the functional microstates, who has given important input during data analyses. We thank Y. Egenolf and M. Stein for programming the IAT in E-prime and U. Bircher, D. Chrobot, N. Gross, L. Hoffmann, E. Meissner, N. Scheurer, and K. Stadler for their help in data collection and processing. This work was supported by Swiss National Science Foundation Grant PP00P1-123381 (to D.K.), and the Mens Sana Foundation (D.K.).

1. Donders FC (1969) On the speed of mental processes. *Acta Psychol (Amst)* 30:412–431.
2. Jensen AR (2006) A brief chronology of mental chronometry. *Clocking the Mind: Mental Chronometry and Individual Differences*, ed Jensen AR (Elsevier, Oxford), pp 1–10.
3. De Houwer J, Teige-Mocigemba S, Spruyt A, Moors A (2009) Implicit measures: A normative analysis and review. *Psychol Bull* 135(3):347–368.
4. Fiske ST, North SN (2015) Measures of stereotyping and prejudice: Barometers of bias. *Measures of Personality and Social Psychology Constructs*, eds Boyle GJ, Saklofske DH, Matthews G (Academic, Elsevier, London), pp 684–718.
5. Stanley DA, Sokol-Hessner P, Banaji MR, Phelps EA (2011) Implicit race attitudes predict trustworthiness judgments and economic trust decisions. *Proc Natl Acad Sci USA* 108(19):7710–7715.
6. Cameron CD, Brown-Iannuzzi JL, Payne BK (2012) Sequential priming measures of implicit social cognition: A meta-analysis of associations with behavior and explicit attitudes. *Pers Soc Psychol Rev* 16(4):330–350.
7. Greenwald AG, Poehlman TA, Uhlmann EL, Banaji MR (2009) Understanding and using the Implicit Association Test: III. Meta-analysis of predictive validity. *J Pers Soc Psychol* 97(1):17–41.
8. Greenwald AG, McGhee DE, Schwartz JL (1998) Measuring individual differences in implicit cognition: The implicit association test. *J Pers Soc Psychol* 74(6):1464–1480.
9. Nosek BA, Hawkins CB, Frazier RS (2011) Implicit social cognition: From measures to mechanisms. *Trends Cogn Sci* 15(4):152–159.
10. Conrey FR, Sherman JW, Gawronski B, Hugenberg K, Groom CJ (2005) Separating multiple processes in implicit social cognition: The quad model of implicit task performance. *J Pers Soc Psychol* 89(4):469–487.
11. De Houwer J (2001) A structural and process analysis of the implicit association test. *J Exp Soc Psychol* 37(6):443–451.
12. Bressler SL (1995) Large-scale cortical networks and cognition. *Brain Res Brain Res Rev* 20(3):288–304.
13. Fuster JM (2006) The cognit: A network model of cortical representation. *Int J Psychophysiol* 60(2):125–132.
14. Mesulam MM (1998) From sensation to cognition. *Brain* 121(Pt 6):1013–1052.
15. Brandeis D, Lehmann D, Michel CM, Mingrone W (1995) Mapping event-related brain potential microstates to sentence endings. *Brain Topogr* 8(2):145–159.
16. Lehmann D, Skrandies W (1980) Reference-free identification of components of checkerboard-evoked multichannel potential fields. *Electroencephalogr Clin Neurophysiol* 48(6):609–621.
17. Lehmann D (1987) *Principles of Spatial Analysis. Handbook of Electroencephalography and Clinical Neurophysiology. Methods of Analysis of Brain Electrical and Magnetic Signals*, eds Gevins AS, Remond A (Elsevier, Amsterdam), pp 309–354.

18. Fleischhauer M, Strobel A, Diers K, Enge S (2014) Electrophysiological evidence for early perceptual facilitation and efficient categorization of self-related stimuli during an Implicit Association Test measuring neuroticism. *Psychophysiology* 51(2):142–151.
19. Forbes CE, et al. (2012) Identifying temporal and causal contributions of neural processes underlying the Implicit Association Test (IAT). *Front Hum Neurosci* 6:320.
20. Hilgard J, Bartholow BD, Dickter CL, Blanton H (2015) Characterizing switching and congruency effects in the Implicit Association Test as reactive and proactive cognitive control. *Soc Cogn Affect Neurosci* 10(3):381–388.
21. Ibáñez A, et al. (2010) Early neural markers of implicit attitudes: N170 modulated by intergroup and evaluative contexts in IAT. *Front Hum Neurosci* 4:188.
22. Coates MA, Campbell KB (2010) Event-related potential measures of processing during an Implicit Association Test. *Neuroreport* 21(16):1029–1033.
23. Egenolf Y, et al. (2013) Tracking the implicit self using event-related potentials. *Cogn Affect Behav Neurosci* 13(4):885–899.
24. Williams JK, Themanson JR (2011) Neural correlates of the implicit association test: Evidence for semantic and emotional processing. *Soc Cogn Affect Neurosci* 6(4): 468–476.
25. Mierke J, Klauer KC (2003) Method-specific variance in the implicit association test. *J Pers Soc Psychol* 85(6):1180–1192.
26. Brendl CM, Markman AB, Messner C (2001) How do indirect measures of evaluation work? Evaluating the inference of prejudice in the Implicit Association Test. *J Pers Soc Psychol* 81(5):760–773.
27. Beer JS, et al. (2008) The Quadruple Process model approach to examining the neural underpinnings of prejudice. *Neuroimage* 43(4):775–783.
28. Gonsalkorale K, Sherman JW, Allen TJ, Klauer KC, Amodio DM (2011) Accounting for successful control of implicit racial bias: The roles of association activation, response monitoring, and overcoming bias. *Pers Soc Psychol Bull* 37(11):1534–1545.
29. Dehaene S, Cohen L (2011) The unique role of the visual word form area in reading. *Trends Cogn Sci* 15(6):254–262.
30. Price CJ, Devlin JT (2011) The interactive account of ventral occipitotemporal contributions to reading. *Trends Cogn Sci* 15(6):246–253.
31. Craig AD (2009) How do you feel–now? The anterior insula and human awareness. *Nat Rev Neurosci* 10(1):59–70.
32. Chen YH, et al. (2009) The temporal dynamics of insula activity to disgust and happy facial expressions: A magnetoencephalography study. *Neuroimage* 47(4):1921–1928.
33. Arnell KM, Killman KV, Fijavz D (2007) Blinded by emotion: Target misses follow attention capture by arousing distractors in RSVP. *Emotion* 7(3):465–477.
34. Hinojosa JA, Méndez-Bértolo C, Pozo MA (2012) High arousal words influence subsequent processing of neutral information: Evidence from event-related potentials. *Int J Psychophysiol* 86(2):143–151.
35. Gallate J, Wong C, Ellwood S, Chi R, Snyder A (2011) Noninvasive brain stimulation reduces prejudice scores on an implicit association test. *Neuropsychology* 25(2): 185–192.
36. Wong CL, Harris JA, Gallate JE (2012) Evidence for a social function of the anterior temporal lobes: Low-frequency rTMS reduces implicit gender stereotypes. *Soc Neurosci* 7(1):90–104.
37. Aflalo T, et al. (2015) Neurophysiology. Decoding motor imagery from the posterior parietal cortex of a tetraplegic human. *Science* 348(6237):906–910.
38. Shackman AJ, et al. (2011) The integration of negative affect, pain and cognitive control in the cingulate cortex. *Nat Rev Neurosci* 12(3):154–167.
39. Simmonds DJ, Pekar JJ, Mostofsky SH (2008) Meta-analysis of Go/No-go tasks demonstrating that fMRI activation associated with response inhibition is task-dependent. *Neuropsychologia* 46(1):224–232.
40. Baumgartner T, Schiller B, Rieskamp J, Gianotti LR, Knoch D (2014) Diminishing parochialism in intergroup conflict by disrupting the right temporo-parietal junction. *Soc Cogn Affect Neurosci* 9(5):653–660.
41. Cikara M, Botvinick MM, Fiske ST (2011) Us versus them: Social identity shapes neural responses to intergroup competition and harm. *Psychol Sci* 22(3):306–313.
42. Baumgartner T, Schiller B, Hill C, Knoch D (2013) Impartiality in humans is predicted by brain structure of dorsomedial prefrontal cortex. *Neuroimage* 81:317–324.
43. Cikara M, Van Bavel JJ (2014) The neuroscience of intergroup relations: An integrative review. *Perspect Psychol Sci* 9(3):245–274.
44. Schiller B, Baumgartner T, Knoch D (2014) Intergroup bias in third-party punishment stems from both outgroup discrimination and ingroup favoritism. *Evol Hum Behav* 35(3):169–175.
45. Wann DL, Branscombe NR (1993) Sports fans - Measuring degree of identification with their team. *Int J Sport Psychol* 24(1):1–17.
46. Greenwald AG, Nosek BA, Banaji MR (2003) Understanding and using the implicit association test: I. An improved scoring algorithm. *J Pers Soc Psychol* 85(2):197–216.
47. Nuwer MR, et al.; International Federation of Clinical Neurophysiology (1998) IFCN standards for digital recording of clinical EEG. *Electroencephalogr Clin Neurophysiol* 106(3):259–261.
48. Pascual-Marqui RD, Michel CM, Lehmann D (1995) Segmentation of brain electrical activity into microstates: Model estimation and validation. *IEEE Trans Biomed Eng* 42(7):658–665.
49. Cacioppo S, Weiss RM, Runesha HB, Cacioppo JT (2014) Dynamic spatiotemporal brain analyses using high performance electrical neuroimaging: Theoretical framework and validation. *J Neurosci Methods* 238:11–34.
50. Rousseeuw P (1987) Silhouettes: A graphical aid to the interpretation and validation of cluster analysis. *J Comput Appl Math* 20:53–65.
51. Michel CM, Seeck M, Landis T (1999) Spatiotemporal dynamics of human cognition. *News Physiol Sci* 14:206–214.
52. Ortigue S, et al. (2004) Electrical neuroimaging reveals early generator modulation to emotional words. *Neuroimage* 21(4):1242–1251.
53. Pascual-Marqui RD (2002) Standardized low-resolution brain electromagnetic tomography (sLORETA): Technical details. *Methods Find Exp Clin Pharmacol* 24(Suppl D): 5–12.
54. Babiloni C, et al. (2009) Judgment of actions in experts: A high-resolution EEG study in elite athletes. *Neuroimage* 45(2):512–521.
55. Knoch D, Gianotti LR, Baumgartner T, Fehr E (2010) A neural marker of costly punishment behavior. *Psychol Sci* 21(3):337–342.
56. Murphy M, et al. (2009) Source modeling sleep slow waves. *Proc Natl Acad Sci USA* 106(5):1608–1613.
57. Nash K, Schiller B, Gianotti LR, Baumgartner T, Knoch D (2013) Electrophysiological indices of response inhibition in a Go/NoGo task predict self-control in a social context. *PLoS One* 8(11):e79462.
58. Pizzagalli D, et al. (2001) Anterior cingulate activity as a predictor of degree of treatment response in major depression: Evidence from brain electrical tomography analysis. *Am J Psychiatry* 158(3):405–415.
59. Schiller B, Gianotti LR, Nash K, Knoch D (2014) Individual differences in inhibitory control–relationship between baseline activation in lateral PFC and an electrophysiological index of response inhibition. *Cereb Cortex* 24(9):2430–2435.
60. Koenig T, Melie-García L (2010) A method to determine the presence of averaged event-related fields using randomization tests. *Brain Topogr* 23(3):233–242.
61. Koenig T, Stein M, Grieder M, Kottlow M (2014) A tutorial on data-driven methods for statistically assessing ERP topographies. *Brain Topogr* 27(1):72–83.
62. Michel CM, et al. (1993) Global Field Power: A 'time-honoured' index for EEG/EP map analysis. *Int J Psychophysiol* 15(1):1–5.
63. Mobascher A, et al. (2009) Fluctuations in electrodermal activity reveal variations in single trial brain responses to painful laser stimuli–a fMRI/EEG study. *Neuroimage* 44(3):1081–1092.
64. Olbrich S, et al. (2009) EEG-vigilance and BOLD effect during simultaneous EEG/fMRI measurement. *Neuroimage* 45(2):319–332.
65. Laxton AW, et al. (2010) A phase I trial of deep brain stimulation of memory circuits in Alzheimer's disease. *Ann Neurol* 68(4):521–534.
66. Zumsteg D, Friedman A, Wieser HG, Wennberg RA (2006) Propagation of interictal discharges in temporal lobe epilepsy: Correlation of spatiotemporal mapping with intracranial foramen ovale electrode recordings. *Clin Neurophysiol* 117(12): 2615–2626.
67. Zumsteg D, Lozano AM, Wieser HG, Wennberg RA (2006) Cortical activation with deep brain stimulation of the anterior thalamus for epilepsy. *Clin Neurophysiol* 117(1): 192–207.
68. Ortigue S, Sinigaglia C, Rizzolatti G, Grafton ST (2010) Understanding actions of others: The electrodynamics of the left and right hemispheres. A high-density EEG neuroimaging study. *PLoS One* 5(8):e12160.
69. Nichols TE, Holmes AP (2002) Nonparametric permutation tests for functional neuroimaging: A primer with examples. *Hum Brain Mapp* 15(1):1–25.
70. Schulz E, et al. (2008) Impaired semantic processing during sentence reading in children with dyslexia: Combined fMRI and ERP evidence. *Neuroimage* 41(1):153–168.
71. Clark VP, Fan S, Hillyard SA (1995) Identification of Early Visual evoked potential generators by retinotopic and topographic analyses. *Hum Brain Mapp* 2(3):170–187.
72. Heinze HJ, et al. (1994) Combined spatial and temporal imaging of brain activity during visual selective attention in humans. *Nature* 372(6506):543–546.
73. Binder JR, Desai RH (2011) The neurobiology of semantic memory. *Trends Cogn Sci* 15(11):527–536.
74. Polich J (2007) Updating P300: An integrative theory of P3a and P3b. *Clin Neurophysiol* 118(10):2128–2148.
75. Desmurget M, Sirigu A (2009) A parietal-premotor network for movement intention and motor awareness. *Trends Cogn Sci* 13(10):411–419.
76. Fried I, et al. (1991) Functional organization of human supplementary motor cortex studied by electrical stimulation. *J Neurosci* 11(11):3656–3666.
77. Hallett M (1994) Movement-related cortical potentials. *Electromyogr Clin Neurophysiol* 34(1):5–13.
78. Thiemann U, et al. (2012) Cortical post-movement and sensory processing disentangled by temporary deafferentation. *Neuroimage* 59(2):1582–1593.

Supporting Information

Schiller et al. 10.1073/pnas.1515828113

SI Materials and Methods

The sLORETA (53) solution space consists of 6,239 voxels (voxel size: 5 × 5 × 5 mm) and is restricted to cortical gray matter and hippocampi, as defined by the digitized Montreal Neurological Institute probability atlas. The sLORETA functional images represent the electrical activity at each voxel as squared magnitude (i.e., power) of computed current density (unit: amperes per square meter, A/m^2). sLORETA computes the electrical neuronal activity without assuming a predefined number of sources. The sLORETA method has received considerable validation from studies combining EEG/MEG source localizations performed in conjunction with other localization methods, such as functional magnetic resonance imaging (63, 64) and positron emission tomography (65). Further, the method has been validated with experimental data that reveal the true generators from invasive, implanted depth electrodes (66, 67) and has been demonstrated to correctly localize deep structures such as the anterior cingulate cortex (58) and mesial temporal lobes (66).

For each subject, we first averaged all scalp maps within each microstate, pooling together the incongruent and the congruent condition, and then estimated the individual sLORETA functional images for each microstate. To identify the neural generators that characterize a particular microstate, we statistically contrasted the individual sLORETA functional images of a specific microstate to the individual sLORETA functional images of the previous microstate (microstate 1 was compared with the 100-ms period before stimulus onset, microstate 2 contrasted with microstate 1). The rationale behind this approach (68) is that we were interested in tracking the temporal dynamic of the distinct mental processes (microstates) in the IAT that lead from perception to action. The localization of the intracerebral sources of each microstate was assessed by whole-brain voxel-by-voxel t tests of the sLORETA images of the log-transformed computed current density power between a particular microstate and the previous one. In the resulting statistical 3D images, cortical voxels were identified as statistically different through a nonparametric approach by using a randomization strategy (69) that determined the critical probability threshold values for the observed t values with correction for multiple testing.

SI Results

Behavioral Results: D scores. We calculated D scores according to the improved scoring algorithm (46). This score represents the difference between mean response latencies in congruent and incongruent trials, divided by the pooled SD across trials. D scores were significantly different from 0 in soccer fans [$M = 0.69$, SD = 0.32, $t(36) = 13.15$, $P < 0.001$, $\eta^2 = 0.83$] and in political supporters [$M = 0.54$, SD = 0.35, $t(45) = 10.71$, $P < 0.001$, $\eta^2 = 0.72$]. Pooling all subjects together, we also obtained a D score that was significantly different from 0 [$M = 0.61$, SD = 0.34, $t(82) = 16.34$, $P < 0.001$, $\eta^2 = 0.77$].

Detailed Description of Cluster Topographies. The topographies of the nine clusters in their sequence of occurrence are shown in Fig. 1*A*. Cluster 1 had a contingent negative variation-like topography, characterized by a central negativity. The topography of cluster 2 showed the characteristic P1 distribution with a bilateral positivity over occipital electrodes. Cluster 3 reflected a bilateral posterior negativity and a frontal positivity. Cluster 4 showed a less pronounced posterior negativity and a developing posterior positivity. A P3-like posterior positivity was definitive in cluster 5. This posterior positivity moved slightly in an anterior direction in clusters 6, 7, and 8. Within the same time range, an anterior negativity developed that reached its maximum in cluster 8. This anterior negativity was still present in cluster 9 together with a right-lateralized positivity. The sequence of early clusters 2–4 strongly resembled early ERP components (also called, P1-N1-P2) related to visual word processing (70), and the overall sequence of the nine clusters was in good agreement with the sequence of scalp topographies shown during another study that used a different version of the IAT (23).

Detailed Description of Source Localization Results. In a final step, we localized the brain sources that characterized the distinct microstates across conditions (Fig. 1*C*; for a detailed overview of activated voxels, please see Table S1, and for time plots of the reported activation clusters, please see Fig. S4). No significant voxels appeared in microstate 1 (all $P > 0.14$). P1-like microstate 2 was characterized by activation in the extrastriate cortex (BA18/19), which is consistent with previous source localizations of the P1 and indicates early visual processing (71, 72). In the following microstate 3 that occurred around 200 ms, a network consisting of the left temporal pole (BA22/38), the left insula (BA13), and the dorsal anterior cingulate cortex (dACC; BA24) was active. The coactivation of these areas (31) and its time of appearance (32) might indicate arousal-related processing. Microstate 4 occurred around 220 ms and was characterized by activity in the lingual gyrus (BA18) and other vision-related occipito-temporal areas. Activity in these regions suggests that lexical perceptual processing of the presented words takes place during this microstate (29, 30). The following, P3-like microstate 5 was characterized by two main activation areas, one in the left temporo-parietal junction (TPJ; BA7/39/40) and another in the precuneus and the posterior cingulate cortex (PCC; BA7/31/39). These areas and the P3 component in general are considered to be involved in attention and memory processes (73, 74). Possibly, after lexical processing during microstate 4, the word is categorized as "ingroup," "outgroup," "good," or "bad" during microstate 5 by accessing previously stored knowledge from memory. The following microstate 6 that occurred in temporal proximity to the button press was characterized by activity in the middle cingulate cortex (MCC; BA23/24/31) and the posterior parietal cortex (PCC; BA40). Activity in these regions suggests that participants implement cognitive control to select the motor response during this microstate (37–39). This finding implies that after participants have mentally assigned the word to a specific category during microstate 5, they now select the motor response that correctly classifies the word. The last microstate before button press, microstate 7, was characterized by activity in motor-related frontal regions, encompassing the premotor cortex, the supplementary motor area (both BA6), and the primary motor cortex (BA4). We postulate that the motor response (i.e., the button press) is prepared and executed during this microstate (75, 76). After the execution of the response, during microstate 8, we again found activation in the (pre)motor cortex (BA4/6). Research shows that motor processing can persist well beyond the motor response (77, 78). Alternatively, this motor-related activity could be explained by the fact that subjects also had to remove their finger from the key.

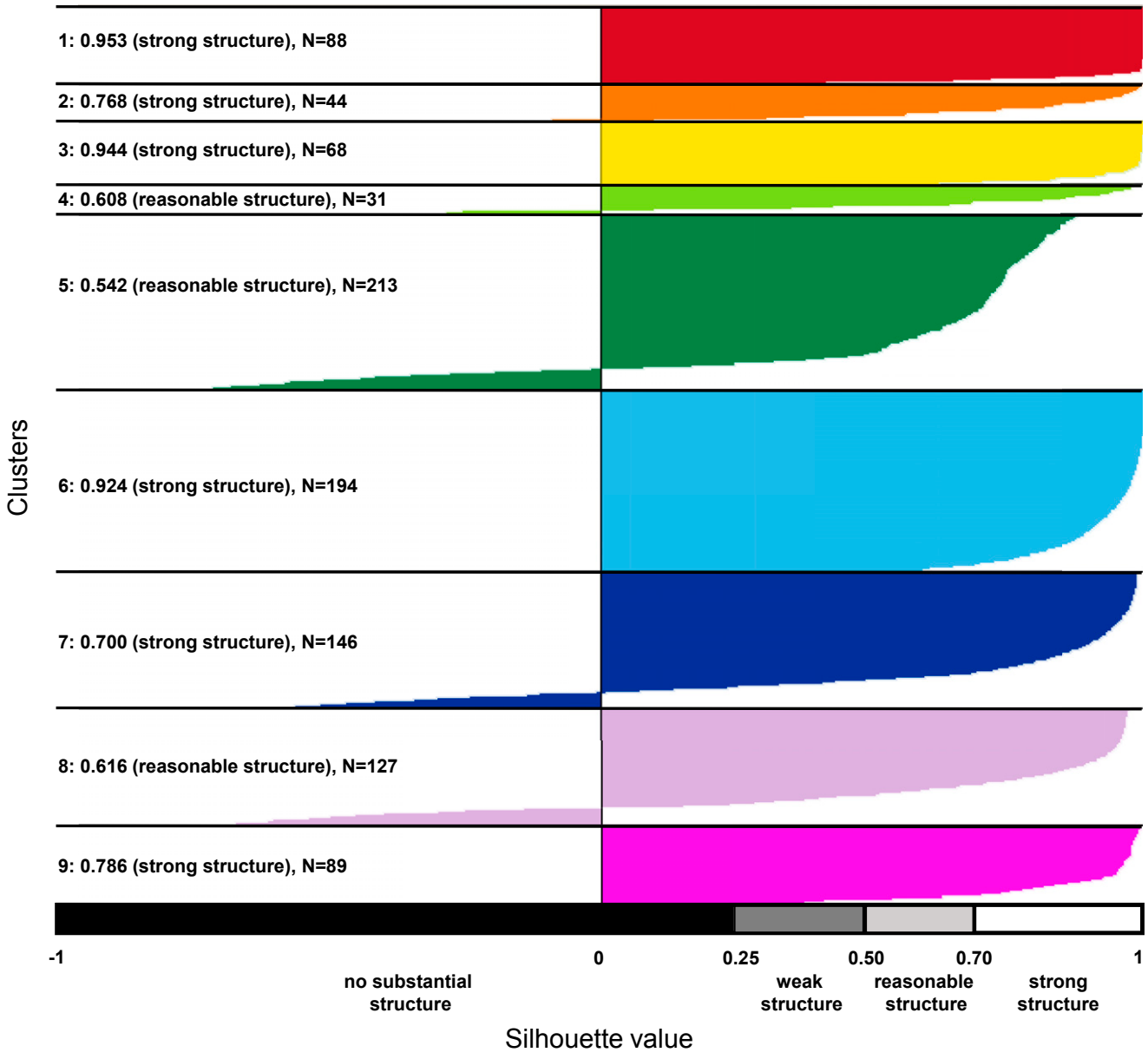

Fig. S1. Silhouette plot for the optimal cluster solution. Plot of silhouette values for the spatial K-means clustering of 1,000 ERP maps (500 grand-mean ERP maps of the congruent condition and 500 grand-mean ERP maps of the incongruent condition). On the *y* axis, all ERP maps belonging to a particular cluster are ordered by decreasing silhouette value. The *x* axis represents the silhouette value. The silhouette value for each ERP map is a measure of how similar that ERP map is to ERP maps in its own cluster, compared with ERP maps in other clusters. The silhouette value can range between −1 and 1. A high silhouette value indicates that the ERP map is well-matched to its own cluster, and poorly matched to neighboring clusters. The average silhouette value and the number of ERP maps for each cluster is given at the left. The empirical interpretation of the average silhouette value for a cluster is shown at the bottom. The colored background corresponds to the cluster assignment shown in Fig. 1*A*. Following the method of Rousseeuw (50), the optimal number of clusters is selected such that a maximum number is obtained while all clusters retain a reasonable structure.

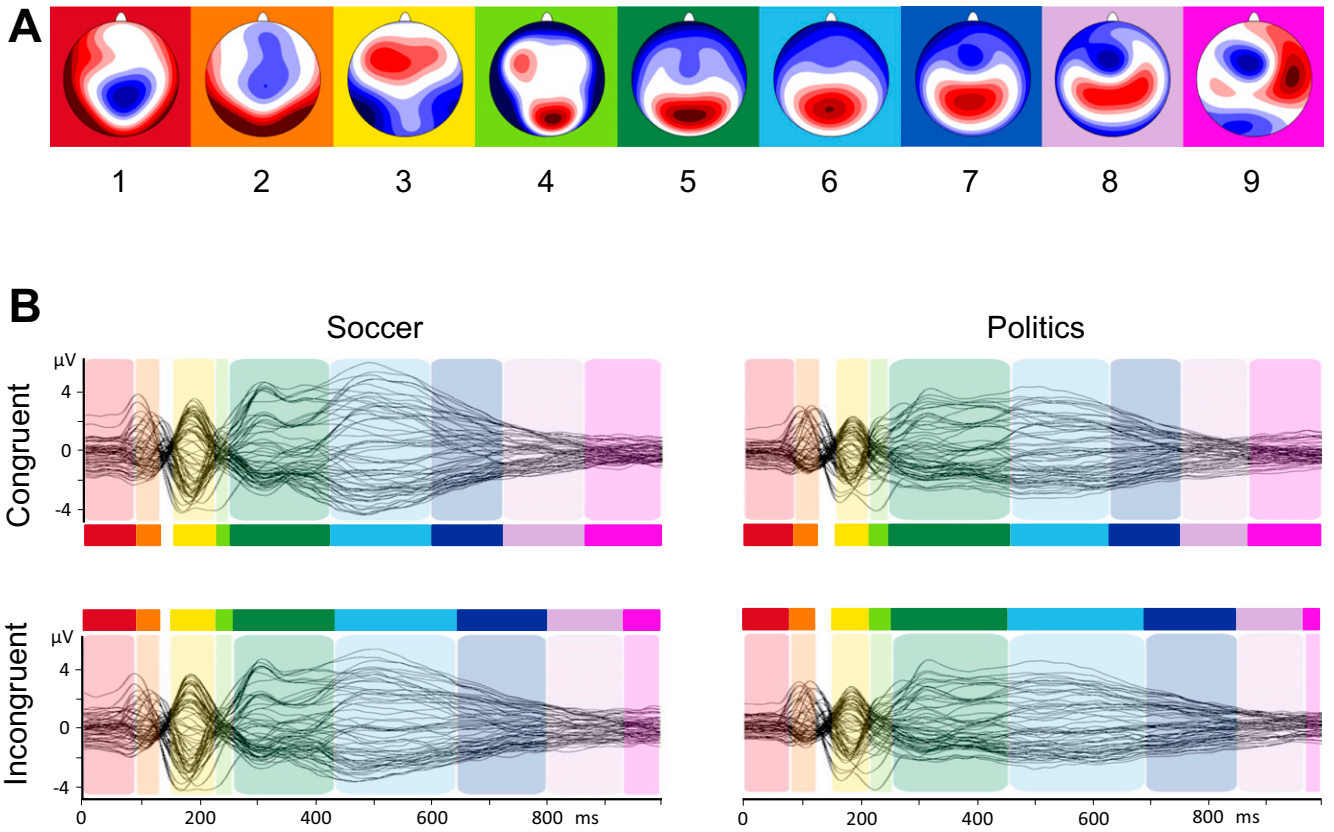

Fig. S2. Microstate analysis of the IAT-evoked ERPs. (*A*) Topographies of the nine microstate clusters in the sequence of occurrence. Head seen from above: Red indicates positive values and blue indicates negative values, referred to average reference. The colored background corresponds to the assignment shown in *B*. (*B*) Results of the spatiotemporal ERP analysis, separately for each condition (rows) and group (columns). The microstates are marked in color on the superimposed grand mean ERP waveforms of all 64 channels for the Soccer-IAT congruent condition (*Upper Left*), Soccer-IAT incongruent condition (*Lower Left*), Politics-IAT congruent condition (*Upper Right*), and Politics-IAT incongruent condition (*Lower Right*). The vertical axis indicates amplitude (in microvolts), and the horizontal axis indicates time (in milliseconds). Please note that the sequence of microstates was identical for both groups and an additional microstate in the incongruent condition did not occur in soccer fans or in political supporters.

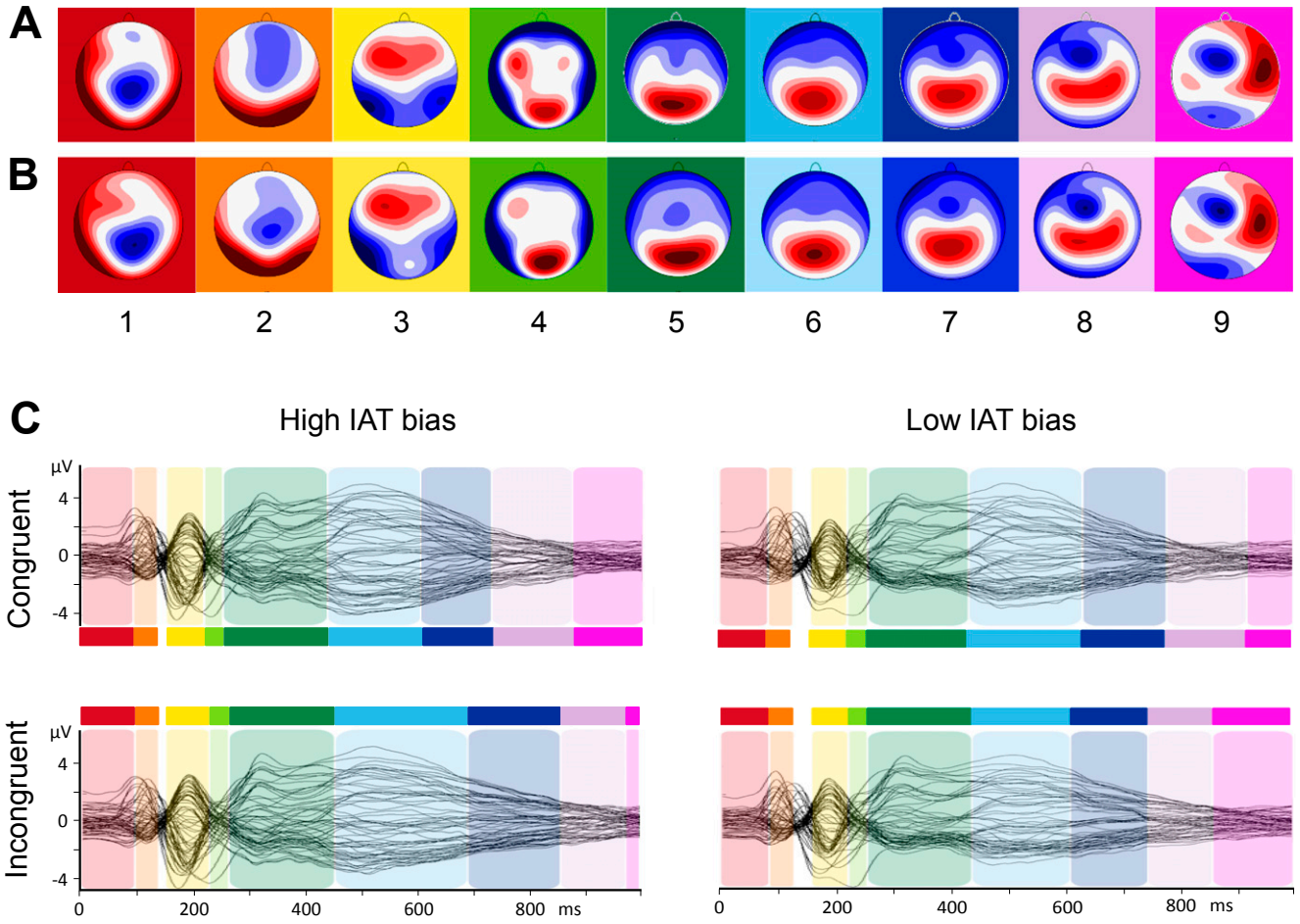

Fig. S3. Microstate analysis of the IAT-evoked ERPs in the groups: High IAT bias ($n = 41$) versus Low IAT bias ($n = 42$). Topographies of the nine microstate clusters in the High IAT bias group (*A*) and in the Low IAT bias group (*B*) in the sequence of occurrence. Head seen from above: Red indicates positive values and blue indicates negative values, referred to average reference. The colored background corresponds to the assignment shown in *C*. (*C*) Results of the spatio-temporal ERP analysis. The microstates are marked in color on the superimposed grand mean ERP waveforms of all 64 channels for the congruent condition of the High IAT bias group (*Upper Left*), for the incongruent condition of the High IAT bias group (*Lower Left*), for the congruent condition of the Low IAT bias (*Upper Right*), and for the incongruent condition of the Low IAT bias group (*Lower Right*). The vertical axis indicates amplitude (in microvolts); the horizontal axis indicates time (in milliseconds).

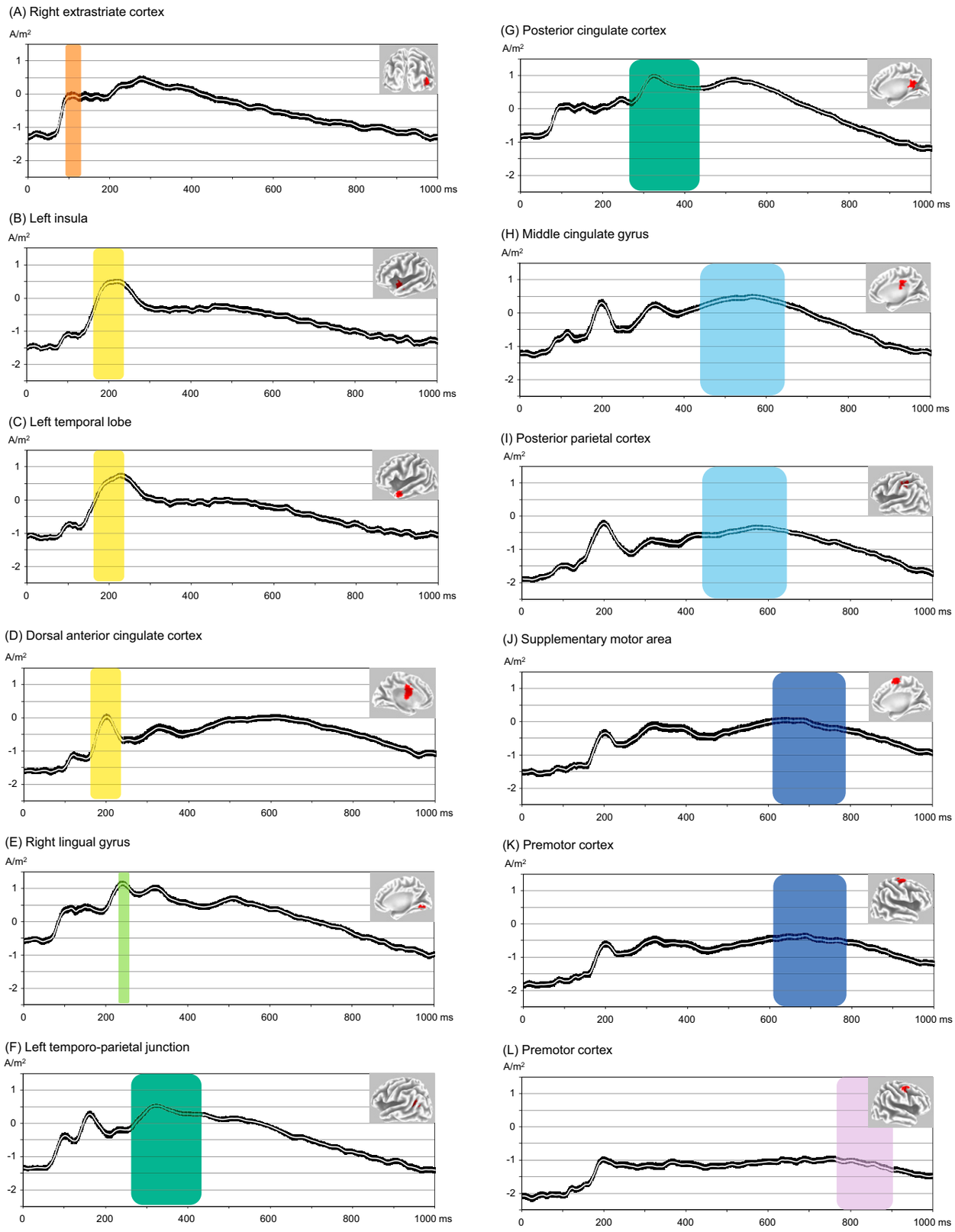

Fig. S4. Time plots main activation clusters of microstates 2–8. Shown in this figure are subject-wise normalized and log-transformed current source density for regions of interest (ROIs; 10-mm sphere around the maximum *t* value) comprising the main activation clusters of microstate 2 [(*A*) Right extrastriate cortex, BA19; $x = 50$, $y = -69$, $z = 7$; MNI], microstate 3 [(*B*) Left insula, BA13, $x = -39$, $y = 5$, $z = -5$; (*C*) Left temporal pole, BA38, $x = -51$, $y = 11$, $z = -21$; (*D*) Dorsal anterior cingulate cortex, BA32, $x = -5$, $y = -5$, $z = 35$], microstate 4 [(*E*) Right lingual gyrus, BA18; $x = 15$, $y = -67$, $z = -3$], microstate 5 [(*F*) Left temporo-parietal junction, BA39; $x = -36$, $y = -59$, $z = 26$; (*G*) Posterior cingulate cortex, BA23; $x = 5$, $y = -52$, $z = 23$], microstate 6 [(*H*) Middle cingulate cortex, BA23; $x = 0$, $y = -25$, $z = 33$; (*I*) Posterior parietal cortex, BA40; $x = -42$, $y = -33$, $z = 44$], microstate 7 [(*J*) Supplementary motor area, BA6; $x = 6$, $y = -2$, $z = 67$; (*K*) Premotor cortex, BA6; $x = 30$, $y = -5$, $z = 65$], and microstate 8 [(*L*) Premotor cortex, BA6; $x = 46$, $y = 1$, $z = 51$]. In black, SEs are shown. Further, the time periods of microstate 2–8 (average of the incongruent and congruent condition) are colored with transparent planes. The colored backgrounds correspond to the cluster assignment shown in Fig. 1*A*.

Table S1. Detailed overview of activated voxels in microstate 2–8

Region	Hemisphere	BA	t_{max}	*x*	*y*	*z*	Voxels
Microstate 2							
Cuneus (extrastriate cortex)	R	19	5.42	30	−90	25	34
Fusiform gyrus	R	37	4.57	35	−55	−15	31
Inferior occipital gyrus (extrastriate cortex)	R	18	4.46	50	−80	−5	10
Middle occipital gyrus (extrastriate cortex)	**R**	**19**	**5.68**	**50**	**−70**	**5**	**49**
Middle temporal gyrus	**L/R**	**39**	**6.05**	**50**	**−70**	**10**	**59**
Parahippocampal gyrus	R	19	4.60	30	−50	−5	13
Precuneus (extrastriate cortex)	R	19	4.85	30	−75	35	25
Superior temporal gyrus	R	39	5.84	50	−55	10	36
Microstate 3							
Cingulate gyrus (dACC)	L	24	4.79	−15	0	40	24
Inferior frontal gyrus	L	47	9.49	−45	15	−5	112
Inferior frontal gyrus	R	44	4.98	50	0	20	11
Inferior parietal lobule	L	40	7.15	−50	−30	25	61
Inferior temporal gyrus	L	20	6.67	−50	0	−35	25
Insula	**L**	**13**	**12.4**	**-40**	**5**	**−5**	**97**
Insula	R	13	5.2	45	−5	15	31
Middle frontal gyrus	L	6	6.19	−35	−10	45	49
Middle frontal gyrus	R	6	5.35	35	−10	45	21
Middle temporal gyrus	L	21	9.55	−50	5	−20	57
Postcentral gyrus	L	43	8.84	−50	−15	15	82
Postcentral gyrus	R	3	6.05	50	−20	45	42
Precentral gyrus	L	44	11.7	−45	0	5	106
Precentral gyrus	R	4	6.35	45	−20	40	99
Sub-gyral	L	13	10.7	−40	0	−10	11
Superior temporal gyrus	**L**	**22/38**	**12.6**	**−45**	**5**	**−5**	**149**
Superior temporal gyrus	R	22/38	4.63	55	0	5	28
Supramarginal gyrus	L	40	5.96	−55	−40	30	13
Transverse temporal gyrus	L	42	7.77	−55	−15	10	16
Microstate 4							
Cuneus	L/R	30	7.16	10	−60	5	23
Fusiform gyrus	R	19	7	25	−60	−15	20
Lingual gyrus	**L/R**	**19**	**7.51**	**15**	**−65**	**−10**	**84**
Parahippocampal gyrus	R	19	7.03	20	−55	−10	20
Posterior cingulate	L/R	30	6.81	5	−60	5	38
Microstate 5							
Angular gyrus (TPJ)	**L**	**39**	**9.58**	**-40**	**-65**	**35**	**16**
Anterior cingulate	L/R	32	4.68	0	35	25	27
Cingulate gyrus (PCC)	**L/R**	**31**	**9.55**	**-10**	**-50**	**40**	**91**
Cuneus	L/R	7	5.84	−5	−70	30	20
Inferior parietal lobule (TPJ)	**L**	**39**	**10.1**	**-35**	**-65**	**40**	**56**
Inferior parietal lobule	R	40	8.32	35	−50	40	108
Insula	L	13	6.37	40	−45	20	10
Medial frontal gyrus	L/R	6	5.67	10	−30	55	72
Middle temporal gyrus	L	39	7.78	−35	−65	25	27
Paracentral lobule	L/R	5	8.19	5	−45	50	85
Postcentral gyrus	L/R	7	7.29	−10	−55	65	127
Posterior Cingulate (PCC)	**L/R**	**31**	**8.43**	**-5**	**-55**	**25**	**32**
Precentral gyrus	L	4	6.05	−15	−35	60	13
Precentral gyrus	R	4	5.13	20	−30	55	12
Precuneus	L/R	19	9.67	-30	-65	40	294
Sub-gyral	L	31	9.24	−20	−50	35	11
Superior frontal gyrus	L/R	6	5.26	−5	30	60	97
Superior parietal lobule (TPJ)	**L/R**	**7**	**10.00**	**-35**	**-65**	**45**	**131**
Superior temporal gyrus	L	39	8.17	−35	−60	30	16
Superior temporal gyrus	R	39	6.98	35	−60	30	33
Supramarginal gyrus	R	40	8.01	40	−50	35	23
Microstate 6							
Cingulate gyrus (MCC)	**L/R**	**23**	**7.16**	**-5**	**-25**	**30**	**144**
Inferior parietal lobule (PPC)	**L**	**40**	**6.22**	**-35**	**-35**	**45**	**46**
Insula	L	13	5.76	−30	−30	20	18
Medial frontal gyrus	L/R	6	4.95	−10	−25	50	16
Paracentral lobule	L/R	31	5.30	−5	−25	45	28

Table S1. Cont.

Region	Hemisphere	BA	t_{max}	x	y	z	Voxels
Postcentral gyrus	L	40	6.13	−40	−30	45	47
Postcentral gyrus	R	2	4.71	50	−25	45	18
Precentral gyrus	L	4	5.80	−30	−30	50	17
Microstate 7							
Anterior cingulate	L/R	32	5.89	10	25	30	29
Cingulate gyrus	L/R	32	5.93	10	30	30	119
Medial frontal gyrus (SMA)	**L/R**	**6**	**6.71**	**15**	**0**	**65**	**160**
Middle frontal gyrus	L	6	5.42	−15	10	65	95
Middle frontal gyrus (premotor cortex)	**R**	**6**	**7.47**	**30**	**-5**	**65**	**116**
Postcentral gyrus	L	3	6.28	−50	−20	60	32
Precentral gyrus ([pre]motor cortex)	**L**	**4/6**	**6.23**	**-35**	**-20**	**70**	**88**
Precentral gyrus ([pre]motor cortex)	**R**	**4/6**	**7.12**	**35**	**-10**	**65**	**54**
Superior frontal gyrus (premotor cortex)	**L/R**	**6**	**7.02**	**30**	**-10**	**70**	**213**
Microstate 8							
Anterior cingulate	L/R	32	5.51	−10	35	20	44
Inferior frontal gyrus	R	44	5.4	50	0	20	19
Insula	R	13	5.46	45	−5	10	22
Medial frontal gyrus	L/R	9	5.19	−10	40	20	31
Middle frontal gyrus (premotor cortex)	**R**	**6**	**5.9**	**50**	**5**	**45**	**64**
Precentral gyrus ([pre]motor cortex)	**R**	**4/6**	**6.31**	**55**	**-5**	**40**	**70**
Superior temporal gyrus	R	22	6.13	65	−5	10	30

Listed in this table are regions with at least 10 significantly activated voxels (5%, two-tailed, whole-brain corrected). Main activation peaks are in bold. BA, Brodmann area of maximum t value(s); region, region as labeled by the sLORETA program (in parentheses: labeling used in the main manuscript); hemisphere, the hemisphere of the cluster is stated (note that bilateral clusters with voxels that were not separated by at least 10 mm were counted as one cluster); t_{max}, maximum t value within a cluster; voxels, number of activated voxels within a cluster; x, y, z, MNI coordinates.

Table S2. IAT stimuli

Positive	Negative	Ingroup (soccer)	Outgroup (soccer)	Ingroup (politics)	Outgroup (politics)
Freude (joy)	Flucht (escape)	FCB [initials]	FCZ [initials]	Politisch links (left-wing)	Politisch rechts (right-wing)
Herz (heart)	Gift (poison)	St. Jakob–Park [stadium]	Letzigrund [stadium]	Ueli Leuenberger [politician]	Christoph Blocher [politician]
Liebe (love)	Hunger (hunger)	Thorsten Fink [coach]	Urs Fischer [coach]	Umweltpolitik (environmental policies)	Zuwanderungbegrenzung (restricting immigration)
Mutter (mother)	Hass (hate)	Franco Costanzo [team captain]	Silvan Aegerter [team captain]	Alternative Energien (alternative energies)	Bewaffnete Neutralität (armed neutrality)
Sinn (meaning)	Panik (panic)				
Sonne (sun)	Streit (conflict)				
Wärme (warmth)	Tod (death)				
Spaβ (fun)	Zwang (compulsion)				
Glück (happiness)	Krieg (war)				

Please note that we individually adapted ingroup/outgroup words according to a participant's preferred soccer club and political party, respectively. Shown here are examples for a FC Basel soccer fan (outgroup: FC Zuerich) and for a left-wing green party supporter (outgroup: right-wing Swiss People's Party). Words in parentheses are English translations, words in brackets describe the word category.